Adaptive control of modal properties of optical beams using photothermal effects

Muzammil A. Arain,[1*] William Z. Korth,[1,2] Luke F. Williams,[1] Rodica M. Martin,[1] Guido Mueller,[1] D. B. Tanner,[1] and David H. Reitze[1]

[1]*Department of Physics, University of Florida, P O Box 118440, Gainesville, Florida 32611, USA*
[2]*Current address: Physics Department, California Institute of Technology, 103-33, Pasadena, California 91125, USA*

[*]*muzamil@phys.ufl.edu*

Abstract: We present an experimental demonstration of adaptive control of modal properties of optical beams. The control is achieved via heat-induced photothermal actuation of transmissive optical elements. We apply the heat using four electrical heaters in thermal contact with the element. The system is capable of controlling both symmetrical and astigmatic aberrations providing a powerful means for *in-situ* correction and control of thermal aberrations in high power laser systems. We demonstrate a tunable lens with a focusing power varying from minus infinity to -10 m along two axes using SF57 optical glass. Applications of the proposed system include laser material processing, thermal compensation of high laser power radiation, and optical beam steering.

OCIS codes: (120.6810) Instrumentation; (010.1080) Adaptive optics; (350. 6830) Photothermal effects

References and links

1. J. D. Foster and L. M. Osterink, "Thermal effects in Nd:YAG Laser," Appl. Opts., 41, 3656-3663, (1970).
2. E. Greninger, "Thermally induced wave-front distortions in laser windows," Appl. Opts., 41, 549-552, (1986).A. E. Siegman, *Lasers*, University Science books, Sausalito, CA (1984).
3. P. Hello and J. Vinet, "Analytical models of thermal aberrations in massive mirrors heated by high power laser beams," J. Phys. France, 51, 1267-1282, (1990).
4. P. Hello and J. Vinet, "Analytical models of transient thermoelastic deformations of mirrors heated by high power CW laser beams," J. Phys. France, 51, 2243-2261, (1990).
5. G. Mueller, R. S. Amin, D. Guagliardo, D. McFeron, R. Lundock, D. H. Reitze and D. B. Tanner, "Method for compensation of thermally induced modal distortions in the input optical components of gravitational wave interferometers," 2002 Class. Quantum Grav. 19 1793-1801.
6. R. Lawrence, D. Ottaway, M. Zucker, and P. Fritschel, "Active correction of thermal lensing through external radiative thermal actuation," Opt. Lett. 29, 2635-2637 (2004).
7. M. A. Arain, V. Quetschke, J. Gleason, L. F. Williams, M. Rakhmanov, J. Lee, R. J. Cruz, G. Mueller, D. B. Tanner, and D. H. Reitze, "Adaptive beam shaping by controlled thermal lensing in optical elements," Appl. Opt. **46**, 2153-2165 (2007).
8. R. Schmiedl, "Adaptive optics for CO_2 laser material processing, " in *2nd International Workshop on Adaptive Optics for Industry and Medicine*, G. D. Love, ed. (World Scientific Publishing Co Pte Ltd, 2000), pp. 32-36.
9. S. Sato, "Liquid-crystal lens-cells with variable focal length," Jpn. J. Appl. Phys. **18**, 1679-1684, (1979).
10. W. L. IJzerman, S. T. de Zwart, and T. Dekker, "Design of 2D/3D switchable displays," SID Symposium Digest, 36, 98-101 (2005).
11. T. L. Kelly, A. F. Naumov, M. Yu. Loktev, and M. A. Rakhmatulin, "Focusing of astigmatic laser diode beam by combination of adaptive liquid crystal lenses," Opt. Commun. 181, 295-301 (2000).
12. I. Kanno, T. Kunisawa, T. Suzuki and H. Kotera, "Development of deformable mirror composed of piezoelectric thin films for adaptive optics," Journal of Selected Topics in Quantum Electronics, vol. 13, no. 2, pp. 155-161, 2007.
13. H. Ren and S.-T. Wu, "Adaptive liquid crystal lens with large focal length tunability," Opt. Express **14**, 11292-11298 (2006).
http://www.opticsinfobase.org/oe/abstract.cfm?URI=oe-14-23-11292

14. T.-Y. Chen, C.- H. Li, J.-L. Wang, C. E. Chiu, and G. J. Su, "A MEMS-based Organic Deformable Mirror with Tunable Focal Length,"*2007 IEEE/LEOS International Conference on Optical MEMS and Nanophotonics*, July 16 (2007), pp. 103-104.
15. M. Smith, P. Willems, Auxiliary Optics Support System Conceptual Design Document, Volume 1 Thermal Compensation System, LIGO-T060083-00-D, http://docuserv.ligo.caltech.edu/docs/public/T/T060083-00/T060083-00.pdf
16. M. A. Arain, V. Quetschke, L. F. Williams, G. Mueller, D. B. Tanner, and D. H. Reitze, "Elements for Future Gravitational Wave Interferometers,' Frontiers in Optics, OSA meeting, San Jose, CA, September 2007.
17. M. A. Arain, V. Quetschke, L. F. Williams, R. Martin, G. Mueller, D. B. Tanner, and D. H. Reitze, "Adaptive Optical Elements for Laser Beam Shaping," US provisional patent, Serial No. 61/086,661, US patent pending.
18. F. P. Incropera and D. P. DeWitt, *Fundamentals of Heat and Mass Transfer*, 5th ed., John Wiley & Sons, USA, (2002).
19. A. E. Siegman, "Defining, measuring, and optimizing laser beam quality", Proc. SPIE 1868, 2 (1993).

1. Introduction

The control of laser beam spatial profiles has become more important with the increased use of lasers in industry, research, and everyday life. Absorption of high-power laser radiation in optical materials deposits heat; the resulting changes in shape and refractive index distort the beam shape as the radiation is transmitted or reflected by the optical element. These distortions act as a lens, producing aberrations that depend on the absorbed laser power and incident spatial profile [1-4]. Consequently, the modal properties of the beam change as a function of incident power. An adaptive optics system that can compensate the distortion or otherwise control the modal properties of the laser beams is highly desirable. Possible applications of adaptive optics includes high power laser interferometers [5-7], laser material processing [8], image processing [9,10], and optical displays [11]. For those applications where mechanical repositioning of lenses is not convenient or even possible, it is desirable to control adaptively the laser beam shape by electrical or optical means. There are a number of solutions available including thermal compensation using negative thermo-optic materials [5], CO_2 induced heating and electrical heating of the elements [6,7], deformable mirrors [12], tunable liquid crystals [13], and MEMS mirrors [14]. For high optical power applications, electrical heating from the perimeter of the optic, using "ring heaters," can easily be used for adaptive compensation by controlling the electrical power delivered to one or more heating elements [15]. These systems have been proposed and are planned to be used in high power laser systems such as Laser Interferometer and Gravitational-wave Observatory [6].

We can extend the concept of symmetric ring heaters to include angular segmentation, allowing the application of heat from localized points on the barrel of the optic. This allows for correction of non-cylindrically symmetric aberrations. The use of quadrant ring heaters to compensate for the astigmatic effects resulting from non-normal incidence mirrors, non-uniform absorption, and birefringence of the materials was introduced by us in Refs. 16 and 17. In this paper, we describe in detail the theory and experimental proof of the concept. Issues related to thermal beam steering, response time, and expected focal range are also discussed.

2. Figure of Merit

We begin by developing a figure of merit that allows us to compare different optical materials. The system consists of an optical element heated from the barrel as shown in Fig. 1. We consider a cylinder of radius a and thickness h in a cylindrical co-ordinate system such that the radial direction of the optical element coincides with the radial coordinate r, with $0 \le r \le a$ and the axial direction of the optical element is along the coordinate z, with $-h/2 \le z \le h/2$. The heater (or a system of radially segmented heaters) is placed on the barrel of the optic in good thermal contact with the optical element.

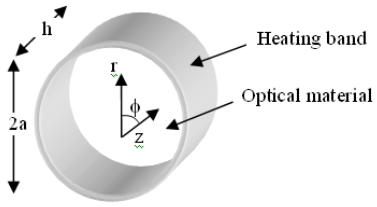

Fig. 1. Geometry of an optical element heated by an external heating band in direct thermal contact with the barrel. This heat can be applied by one or multiple elements positioned along the perimeter of the optical element.

The thermal diffusion equation describing the temperature distribution of the optical element is:

$$\rho C \frac{\partial T}{\partial t} = k\nabla^2 T + Q \qquad (1)$$

where ρ is the density of the material (kg m^{-3}), C is the specific heat (J kg^{-1} K^{-1}), $T(t,r,z,\phi)$ is the temperature (K), t is the time (s), k is the thermal conductivity (W m^{-1} K^{-1}), ∇ is the gradient operator, and Q (W m^{-3}) is the heat generated per unit volume in the optical element. Equation 1 can be solved for both steady-state and transient solutions. In the steady state, Eq. 1 becomes:

$$k\nabla^2 T + Q = 0 \qquad (2).$$

In addition to the generation (or absorption) of heat within the optical element, there will be a heat flux incident on (or radiated from) the surfaces of the optical element. We break the heat flux q (W m^{-2}) into two parts:

$$q = q_{rad} + q_{ext} \qquad (3)$$

where q_{ext} is the known heat flux supplied by the external heaters while q_{rad} is the heat flux radiated back into the surroundings. According to the Stefan-Boltzmann law:

$$q_{rad} = \varepsilon\sigma\left(T^4 - T_{amb}^4\right) \qquad (4)$$

where σ is the Stefan-Boltzmann constant (5.67×10^{-8} W m^{-2} K^{-4}), ε is the emissivity of the material (unit less), and T_{amb} is the ambient temperature. Because the temperature T enters with the 4th power, Eq. (2) becomes a non-linear partial differential equation. The problem-specific boundary conditions are:

$$-k\frac{\partial T}{\partial r}(a,z,\phi) = -\varepsilon\sigma T^4 + q(a,z,\phi), \qquad (5)$$

$$-k\frac{\partial T}{\partial z}(r,-h/2) = \varepsilon\sigma T^4, \qquad (6)$$

$$-k\frac{\partial T}{\partial z}(r,h/2) = \varepsilon\sigma T^4. \qquad (7)$$

The simultaneous solution of Eqs. (2) and (5-7) will provide the steady state temperature distribution in the optical element heated by external heaters in thermal contact with the barrel of the optical element. Similarly, a transient solution can be obtained from Eq. (1).

However, we can simplify the solution considerably by assuming that the temperature distribution depends only on the radial coordinate. Then, the temperature distribution of a cylinder under constant heat load at the barrel is [18]:

$$T(r) = q_{ext}\frac{a^2}{4k}\left(\frac{r^2}{a^2} - 1\right) + T_0, \qquad (8)$$

where T_0 is the temperature and q_{ext} the heat flux at the barrel of the optical element. Note that the solution in Eq. 8 is approximate as it ignores the temperature dependence in the axial direction. Nevertheless, Eq. 8 shows how i) the temperature depends inversely upon the thermal conductivity of the material, and ii) a thermal gradient exists in the radial direction. This thermal gradient $\Delta T = T(r) - T(0)$ will induce through the temperature dependence of the refractive index a lens-like profile in the optical element. The power of this lens depends upon the optical properties of the material. The induced optical path length change ΔOPL is:

$$\Delta\mathrm{OPL} = -h\left[\frac{dn}{dT} + \alpha_T(1+\upsilon)\times(n-1)\right] q_{ext}\frac{r^2}{4k}, \qquad (9)$$

where υ is Poisson's ratio, n is the refractive index of the material, α_T is the coefficient of thermal expansion, and *dn/dT* is the thermo-optic coefficient. Inclusion of υ in Eq. 9 signifies that the barrel of the optical element is constrained and cannot expand radially. Equation 9 also represents a gradient index lens equation that can be described as a lens of focal length *f*:

$$f = \frac{-4k}{h\left[\frac{dn}{dT} + \alpha_T(1+\upsilon)\times(n-1)\right]}\frac{1}{q_{ext}}. \qquad (10)$$

The quantities used in Eqs. 9 and 10 are listed in Table 1 for a number of materials. Eq. 10 provides a figure of merit (*FOM)* representing the strength of the lens produced for a given geometry and incident heat flux. This *FOM,* which gives an easy way to compare optical materials, is:

$$FOM = \left[\frac{dn}{dT} + \alpha_T(1+\upsilon)\times(n-1)\right]\Big/k \qquad (11).$$

It should be noted that the actual temperature dependence requires a solution of Eq. 2 satisfying the boundary conditions. Equations 8-10 are stated here for the purpose of comparing material properties and not for the absolute determination of focal power. Based upon *FOM* values, we have chosen to use SF57 glass in our device. We use COMSOL™, a finite element code, to model our specific geometry, which we compare with experiment below.

Table 1: Material properties of prospective optical elements for adaptive beam shaping

Property	Unit	Fused Silica[(a)]	SF57	BK-7	KDP
Refractive Index *n* @ 1064 nm	-	1.45	1.81	1.50	1.49
d*n*/d*T*	10^{-6} K^{-1}	8.7	6.8	1.5	-48
Thermal Conductivity *k*	W m^{-1} K^{-1}	1.37	0.62	1.11	2.1
Thermal Expansion α_T	10^{-6} K^{-1}	0.55	9.2	8.3	44.0
Absorption Coefficient a	ppm/cm	2.0	<200[(b)]	<1000	250
Poisson's ratio ν	-	0.17	0.248	0.206	0.119
FOM	μm/W	6.3	25.1	4.9	-11.3

[(a)]Corning 7980, [(b)]Experimental data

3. Experimental demonstration

The experimental arrangement is shown in Fig. 2 and 3. The sample is a 1.0 cm long by 2.5 cm diameter SF57 glass disk (a flint glass produced by Schott™ USA) with four symmetrically positioned independent heating elements in thermal contact with its barrel (Fig 2). To minimize conductive heating losses and maximize efficiency, the holder is made of Teflon®, a very low conductor of heat. The SF57 is placed in a vacuum chamber to eliminate convection cooling effects. The dominant heat transport mechanism is radiation; in addition, a small amount of heat is lost via conduction from the holder on which the SF57 is mounted. The heater pads are obtained from Minco Inc. and consist of nichrome wire sealed in Kapton. These heaters can be heated to 200^0 C, and are attached to the SF57 barrel by copper tape. The heaters are connected via copper wires brought outside the vacuum using electrical feedthroughs. There we use four independent power supplies to control the heating. The heaters have a resistance of 25 Ω and thus can be connected to fairly ordinary power supplies.

To characterize the heat-induced thermal lensing in SF57, we use a probe beam that passes through the SF57 via windows in the vacuum chamber. This probe beam is a 10 mW, 1.064 μm Nd:YAG laser, expanded to provide a nearly collimated (large Rayleigh range) 2 mm radius beam waist ($1/e^2$ intensity) at the SF57 sample. The probe beam, after passing through the SF57 and exiting from the vacuum chamber, is divided into two beams. One part passes through a 1 m focal length spherical lens. This lens reduces the beam radius at its focal plane to about 100 μm. A CCD camera (WinCAM) installed on a rail is used to scan the beam in the axial (z) direction. The beam passes through a waist whose location and size depends upon the combination of the heat-induced SF57 thermal lens and the f =1 m static lens. As the focal length of the thermal lens in SF57 changes, the beam waist size and location change. This change is measured by performing successive beam scans using the CCD camera. The analysis software associated with the camera provides Gaussian fits to the beam size at each axial (z) location. The thermal lens is computed by experimentally performing an axial beam scan of this beam and using standard ABCD matrices to calculate the thermal lens as a function of heating power.

The beam splitter sends the other portion of the beam to a 4-quadrant photodetector (QPD). This beam does not pass through any lens. The QPD is capable of measuring small beam angular deviations by measuring the differential power in the right and left halves for horizontal displacements and in the top and bottom halves for vertical displacements. Measurements of the distance between the QPD and SF57 and the displacement in the QPD plane provide the angular displacement induced by the heat-induced lens in the SF57.

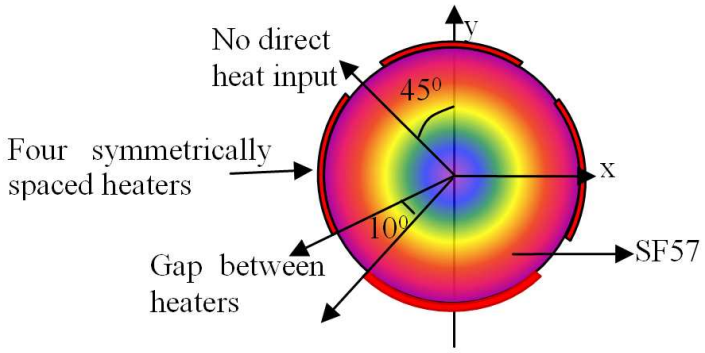

Fig. 2. Schematic diagram of SF57 with four independent heaters arranged symmetrically along the barrel of the optics. Here the direction marked as "No direct heat input" shows the axis of the gap between heaters.

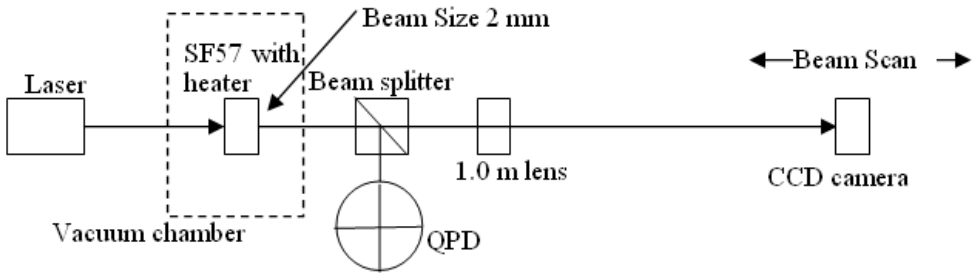

Fig. 3. Experimental setup to measure the thermal lensing of SF57 as a function of the applied heat. The four quadrant photodetector (QPD) is used to measure the beam angular drift. The beam scan gives an estimate of the thermal lensing by measuring the beam waist position and size and using ABCD matrices.

3.1 Thermal lensing dynamic range test

The first series of tests were performed to check the linearity of the system. We varied the power of the heaters from 0 to 2.4 W. This power produces a 200^0C temperature at the barrel of the optic. This temperature is the upper rating of the heaters, so the heating input was not increased further. This limitation does not apply to the SF57, which could be used at higher temperatures with different heaters. The temperature of the system was monitored by a thermocouple *in situ* as well as by an external IR thermal viewer for temperature profiling of the SF57 surface outside the vacuum. The scan data are shown in Fig. 4 for the *X* (horizontal) axis at each axial (Z-axis) location. Because the same power level was used for the vertical axis (top and bottom heaters), similar behavior was observed for *y*. The fitted M^2 values do not change with power [19].

The extracted thermal lens from these measurements is shown in Fig. 5. Here we have also plotted the COMSOL generated cumulative OPL change on the left axis in blue. These results were obtained by using the 3-D temperature distribution and integrating along the axial direction to obtain the *OPL*. The temperature distribution was obtained by solving Eqs. 1-7 numerically using COMSOL. The OPL is then converted to focal length and plotted on the right y-axis along with the measured values. The measured data is in good agreement with the simulation. The only free parameter used in the calculation is the temperature dependence of the thermal conductivity of SF57, which is not known to us. A value close to that for fused silica has been used. At the full heating power of 2.4 W per heater, a lens of -10 m focal length is obtained. Thus, the system focal length can be tuned from infinity to -10 m for 9.6 W of total heating power.

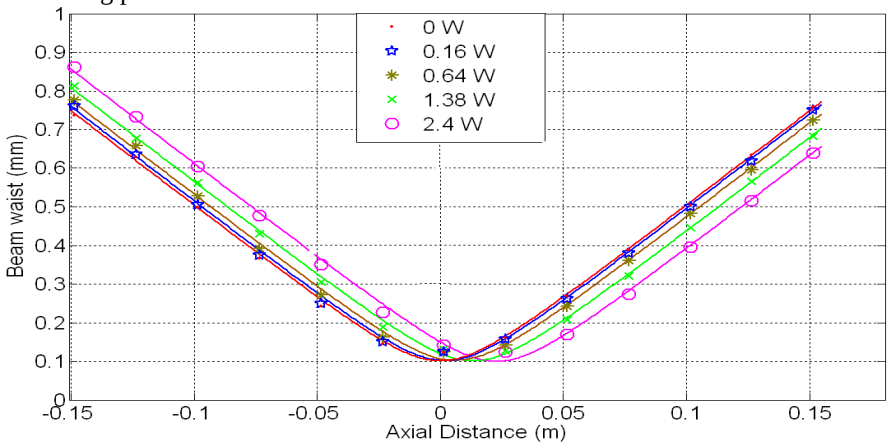

Fig. 4. Beam z-scans for various heating powers. The solid lines are fits to the data points using Gaussian beam parameters. These fits are used to estimate the focal point shift enabling extraction of the induced focal length.

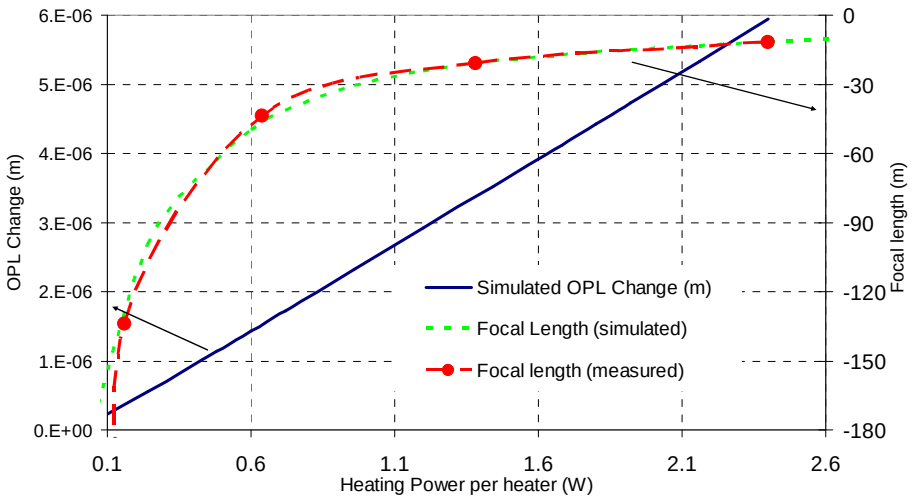

Fig. 5. Computed lensing based upon the z-scan data calculated by means of ABCD matrices. The solid blue line shows the cumulative *OPL* change between the center and the edge of the lens while the dotted green line shows the simulated (using COMSOL) focal length (m) as a function of heating power. The measured data, shown as red points (with error bars) agrees well with the simulations.

To verify further the numerical solution and the data, we obtained a thermal image of SF57 under full heating power with the thermal imaging camera (window limitations required this measurement to be done in air). The heat input was 2.4 W applied to each heater. The temperature data and the COMSOL simulation agree well, as shown in Fig. 6. Also, the isotherms do indeed show a circularly symmetric temperature profile near the center, where the laser beam passes.

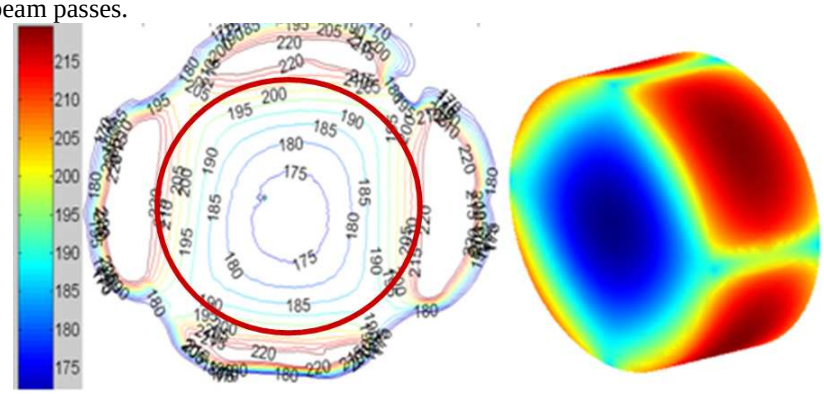

Fig. 6. A thermal image of the SF57 sample and its four heaters with 2.4 W per heater is shown on the left. Contours of constant temperature are indicated. A calculation from COMSOL is shown on the right.

3.2 Astigmatic lens creation

One of the most powerful capabilities of this adaptive lens system is its ability to correct astigmatism (or to provide different focal lengths in the horizontal and vertical axes). This effect is achieved by differentially heating the SF57 in the *x*- or *y*-axes, resulting in the creation of two cylindrical lenses with their axes perpendicular to each other. The focal length of the two lenses can be controlled over a range of infinity to -8 m and -9 m in *x* and *y* axes

respectively. Images taken at a fixed distance from the SF57 sample location are shown in Fig. 7. The inferred thermal lens along the horizontal and vertical axes are given in Table 2.

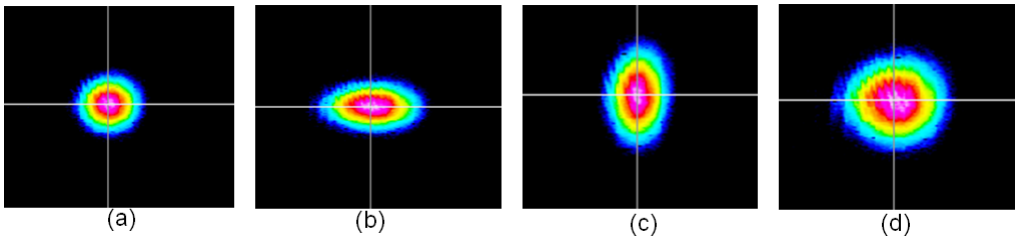

Fig. 7. Astigmatic lens generation using differential heating in SF57. Images of the beam taken at a fixed location show a) cold SF57, b) heating in the *x*-axis only, c) heating in the *y*-axis only, and d) heating in both axes.

Table 2: Astigmatic Lens Creation in SF57 via Differential Heating

Heating	Horizontal Direction			Vertical direction		
	Thermal Lens (m)	Beam Size (mm)	TEM_{00} (%)	Thermal Lens (m)	Beam Size (mm)	TEM_{0} $_{0}$ (%)
No heating	Infinity	345±1	95±1	Infinity	330±1	95±1
Horizontal heating	-8±1	1060±2	94±1	30±2.8	563±1	96±
Vertical heating	27±3	625±1	96±1	-9±1	902±2	94±1
Symmetrical heating	-12±1.2	967±2	93±1	-13±1.2	829±2	94±1

An important feature that can be observed from Table 2 is the cross coupling between the horizontal and vertical axes; i.e., a positive thermal lens is observed in the axis orthogonal to the heat axis. As an example, when a *y*-oriented thermal lens of -9 m is generated via heaters in the vertical direction, a 27 m focal length positive lens is measured in the *x* orientation. This behavior is due to the finite extent of the heaters. The heater geometry shown in Fig. 2 has been modeled in COMSOL and the result of applying heat in vertical direction only is shown in Fig. 8. The data clearly show that, due to the finite heater size, a positive gradient (lower temperature at the edges) appears in the horizontal. However, this lens is weaker than the thermal lens generated on the axis to which heat is applied. This effect also manifests itself in the difference between thermal lensing in a particular axis when heat is applied only in one axis versus the case when heat is applied in both axes. For example, when the maximum heat is applied in both axes, the thermal lens has a focal length of -13 m whereas when the heat is applied in one direction only the thermal lens in that direction is -9 m.

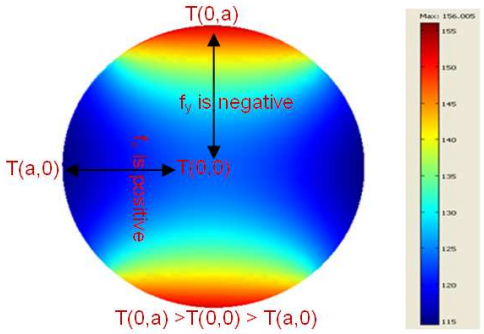

Fig. 8. Simulation of the temperature profile of SF57 with heating in the vertical direction only. Note the negative temperature gradient in the vertical direction where the heat is applied and the positive gradient appearing in the horizontal direction. This is attributed to the finite extent of the heaters. Here f_x and f_y represent focal length values in the *x* and *y* axes.

This cross coupling can be reduced by ensuring that the heaters cover the maximum possible area on the barrel of the optics. The maximum possible area for a single heater is limited by the fact that independent control of each heater is desirable. We simulated the effect of the gap between two adjacent heaters on the cross coupling between x and y directions. We applied heat in the y-direction and measured the integrated OPL in both directions. If there were no cross coupling, then the OPL along x-direction would be zero. Figure 9 shows three data sets for 0, 10, and 20 degree gaps between the adjacent heaters. Heat input to the y-direction heaters was adjusted to provide same OPL in the y-direction. The x-direction OPL is also shown. It is evident that the cross coupling can not be made zero but it can be reduced somewhat by decreasing the gap between the heaters. Going from a 20 degree gap to 0 degree gap, reduces the coupling from --0.44 to -0.33 where the coupling coefficient is defined as $\left(\frac{OPL_x(4mm)-OPL(0)}{OPL_y(4mm)-OPL(0)}\right)$. We selected 4 mm radial distance as more than 99% of the energy in the probe beam is contained in this area.

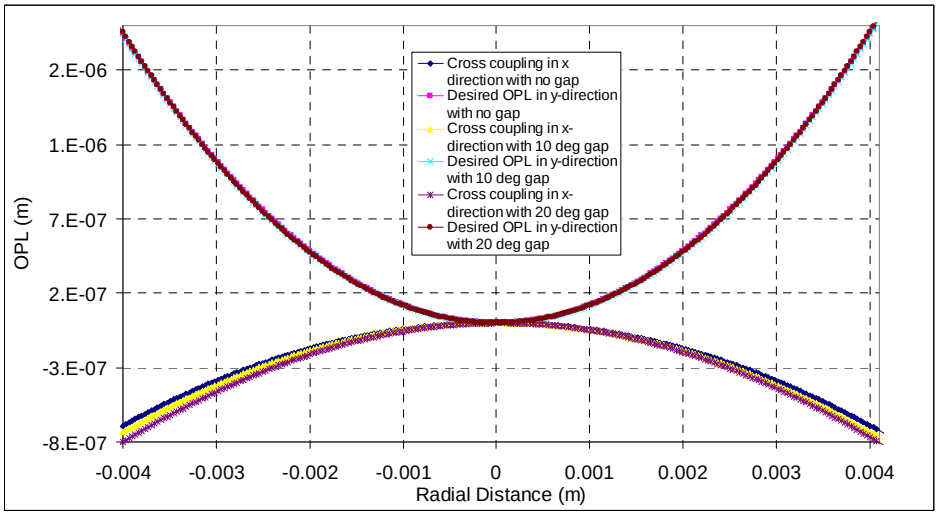

Fig. 9: simulation showing the effect of the gap between adjacent heaters on the cross coupling between the two axes when heat is applied to one direction only.

3.3 Response time

We characterize the response time of the system by measuring the beam size as a function of time. These data are shown in Fig. 10, where we plot the beam size at a fixed location as a function of time after the application of heat. The data cover the whole set of heating values shown in Fig. 4, i.e., for the cold case and for four heating powers. The thermal lens generated in the SF57 depends upon the measured beam difference defined as $\Delta\omega(t)=\omega_f(t)-\omega_i$ where ω_f and ω_i are the final and initial beam sizes. In the steady state, $\Delta\omega(t)$ becomes $\Delta\omega_{ss}=\omega_{f_{ss}}-\omega_i$. We define the response time as the time beam takes to change size from 10% to 90% of $\Delta\omega_{ss}$, excluding the first occurrence of the 90% beam size change caused by the overshoot. The response time of the adaptive device is found to be approximately 500 s.

The response time is also reproduced in the COMSOL simulation. We evaluated the optical path length change evolution at two points; at the center and at a point 2 mm away from the center. Because the beam size at the SF57 sample is 2 mm in radius, this position corresponds to *OPL* change across the beam spot. We can determine the response time of the system from the transient response of the *OPL* change. This response is shown in Fig. 11

where the green and the blue lines represent the simulated *OPL* change as a function of time for positions 2 mm off center and at the center of the SF57 sample respectively. Note that the thermal lensing only depends upon the radial *OPL* change and not on the absolute value of the *OPL*. The red curve shows the *OPL* difference (multiplied by 100X) between the green and the blue curves. The response time is approximately 600 s, in adequate agreement with measurement. The reason for the large overshoot is due to the low thermal conductivity of the SF57. When the heat is applied to the edge of the optic, the temperature of the edge starts rising instantly because it is in thermal contact with the heater. However, the heat takes some time before it reaches the center. Therefore a larger gradient between the edge and the center is developed initially. However, as the heat diffuses toward the center of the optic, the gradient decreases.

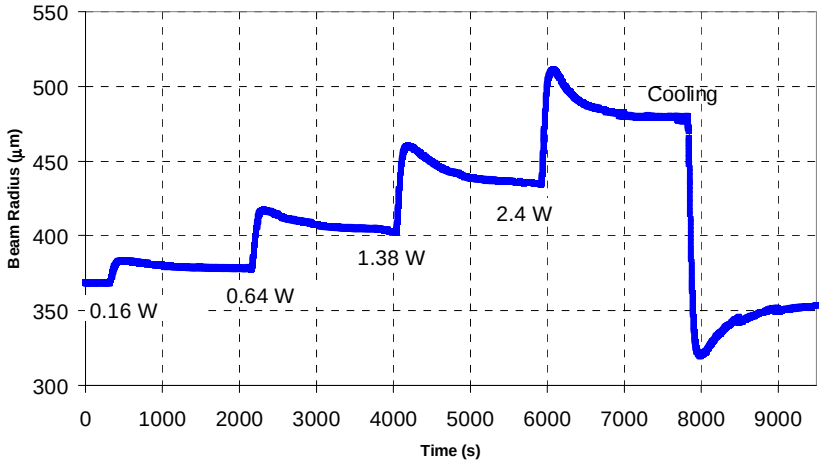

Fig. 10. Beam waist measured at a fixed location for various degrees of SF57 heating. The response time is measured as the average of five step changes and is found to be 500 ± 80 s calculated as average of the response time during four heating cycles and one cooling phase.

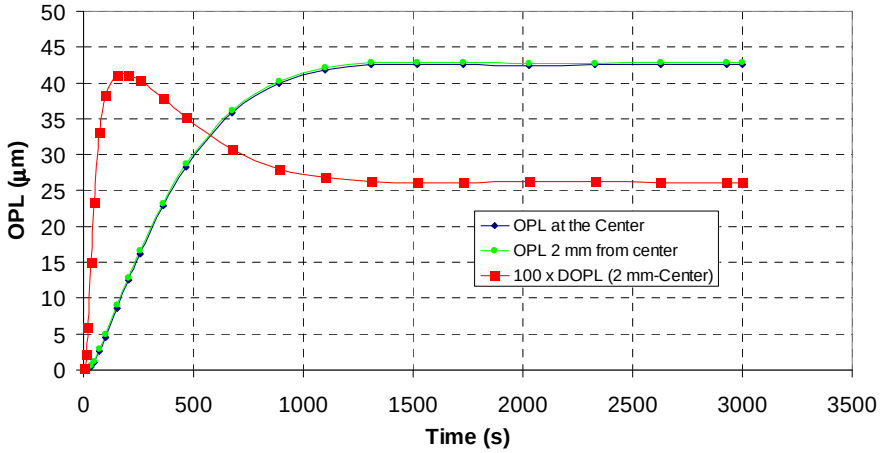

Fig. 11. Simulation of the heating response showing the OPL change at two points—the center of the SF57 and a point 2 mm away from the center, corresponding to 2 mm waist beam size. The difference is shown as the red curve multiplied by 100.

3.4 Thermal beam steering

The application of heat may produce some power-dependent beam steering from either off-axis beam propagation or asymmetries due to differences among the heating segments. If the centering of the beam is not perfect, the steering can be corrected through differential heating of the various parts of the SF57. The QPD shown in Fig. 3 is used to measure the thermally-induced beam steering. The beam size at the QPD was approximately 2.5 mm in diameter. In Fig. 12, we plot the measured beam displacement (normalized to the beam size) as a function of time as heat is applied to various combinations of the segmented heaters. Here, both horizontal and vertical thermal beam drift has been measured. Each block in Fig. 12 represents a specific state of SF57 heating as indicated in the plot. We start by turning all heaters to the 'ON' state (full heating power). The bottom heater is turned ON at a slightly later stage. This delay does show up as beam drift in the vertical direction. Once all heaters are turned ON, the beam drift is less than 0.01% of the beam size. This level of beam drift corresponds to 0.25 μradian angular deviation. This small amount observed could actually be due to a slight misalignment in the vertical direction. For the horizontal beam drift, there is almost no change from the cold to the hot case.

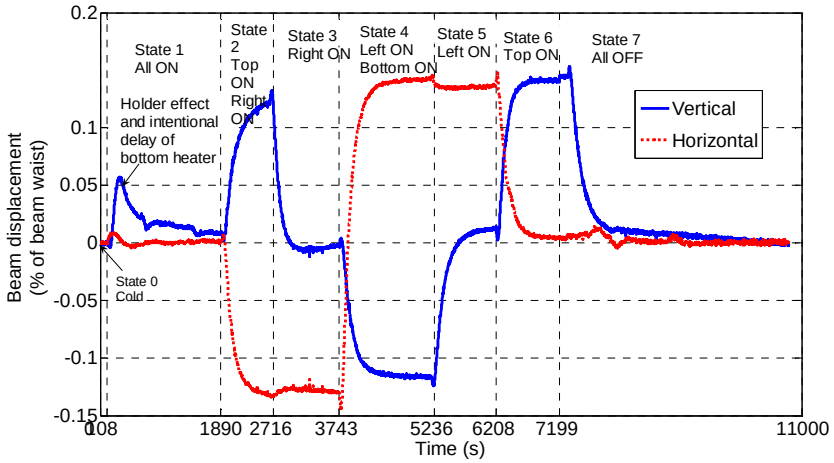

Fig. 12. Beam drift in the horizontal and vertical directions. The *y*-axis deviation is scaled to the 2.5 mm beam size at the QPD and shown as a percentage—a 0.1% deviation corresponds to a 2.5 μm shift. Various states of the SF57 heater are shown as separate grid blocks. The response time is on the order of 500 seconds calculated as average of the response time during four heating cycles and one cooling phase.

Fig. 12 illustrates another use for the system: high resolution beam steering. This effect demonstrated by selectively turning the heat ON as shown in separate grid blocks. For example, state 2 represents the case when the beam is steered diagonally by turning the left and bottom heaters to the OFF state. Various combinations of heating control show that the beam can be effectively steered in all directions. The range of the available steering is low; moreover there is also deviation of about 0.15% on the beam size if 2.4 W of heating is applied to one of the heaters. Thus, one should be careful in using this mechanism in steering applications. Coupled with the steering will be second-order phase front changes.

3.5 Beam quality

The quality of the thermal lens is also important to investigate. We have shown beam scan data in Fig. 4 that shows virtually no change in the M^2 value as compared with the original

beam. The M^2 value remains at 1.20±0.01 for all cases of heating as well as for no heating. In addition, we took beam profile measurements and monitored the TEM_{00} Gaussian content of the beam. There is no noticeable change in the TEM_{00} Gaussian content of the beam. This process was done for various beam sizes starting from 1 to 5 mm, with no noticeable degradation observed after the beam passed through SF57 thermal lens.

One possible concern with the experimental realization of the adaptive lens comes from the lack of rotational heating symmetry and possible non-uniformity. Figure 2 shows the configuration, with a gap between two adjacent heaters, making the temperature at the perimeter of the SF57 vary as a function of angle. This behavior is evident from measured and simulated data in Fig. 6, where the temperature at the barrel is lower in the gaps between the heaters, i.e., at 45^0 to the heater central axis. To show this more clearly, we have plotted in Fig 13 the temperature profile along the heating axis and along the 45^0 line. (See Fig. 2.) This plot represents the worst case of unintended astigmatism generated via SF57 heating. There is no difference in the temperature profile within the central 4.5 mm radius. Thus, this is not a fundamental limitation of the experiment, although it could be rectified by using heaters that have more angular extent.

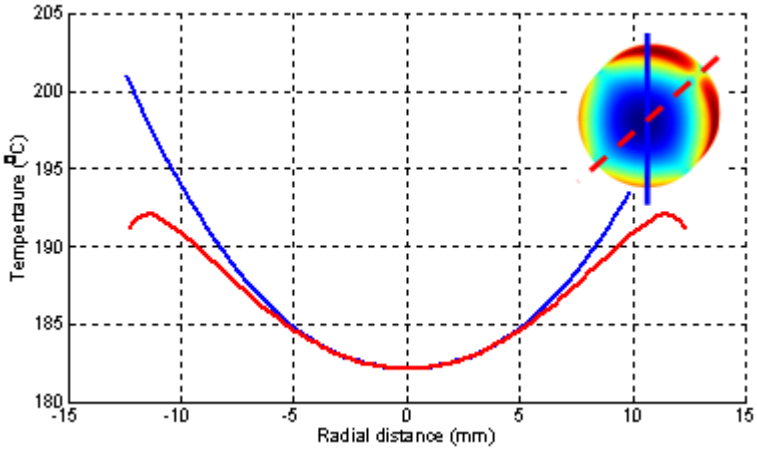

Fig. 13. Temperature profile across the center line of the heating elements in y-direction and 45^0 to the axis of the heating elements.

The lens created by heating the barrel in a particular radial direction is very close to an ideal lens. This fact can be shown by taking a slice through a particular axis and fitting a quadratic function to the profile. Fig. 14 shows a cross-section of the measured temperature distribution along the *y*-axis using a thermal IR camera. Here we have also plotted the residuals to the quadratic fitting equation. It can be seen that the residues are well within the $\pm 1^0$C resolution of the thermal camera.

There could be concerns about non-linearity of optical properties of materials at elevated temperature. However, it should be noted that the temperature differential across the optic is much smaller compared to the increase in over-all temperature of the optic. We simulated the temperature rise as well as the resultant integrated OPL in COMSOL. The results are shown in Fig. 15. Here it is clear that the temperature profile and the OPL both have same regression coefficient. Therefore, it can be inferred that if the temperature profile is quadratic, the resultant OPL will also be quadratic as well.

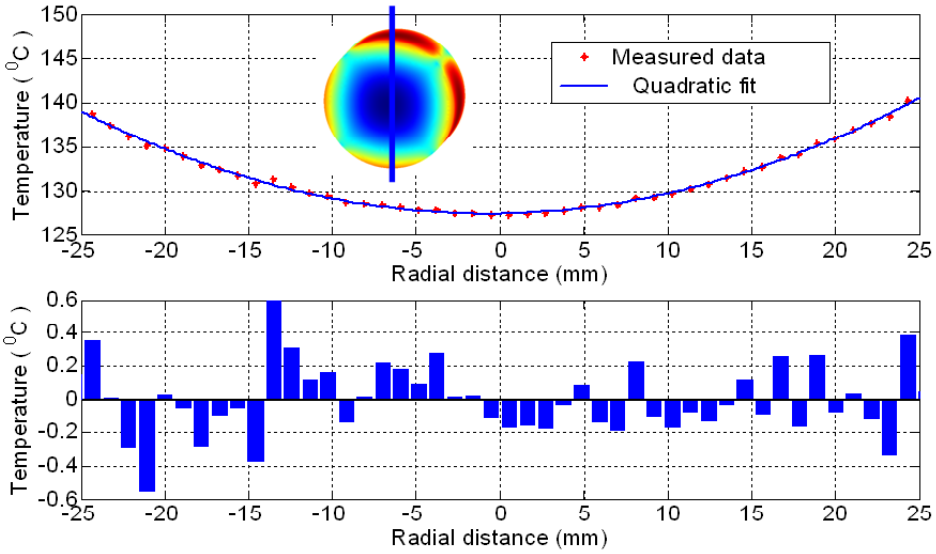

Fig. 14. Measured temperature profile across the center line of the heating elements in the *y*-direction and a quadratic fit to the data. The lower graph shows the residues of the quadratic fit to the measured data.

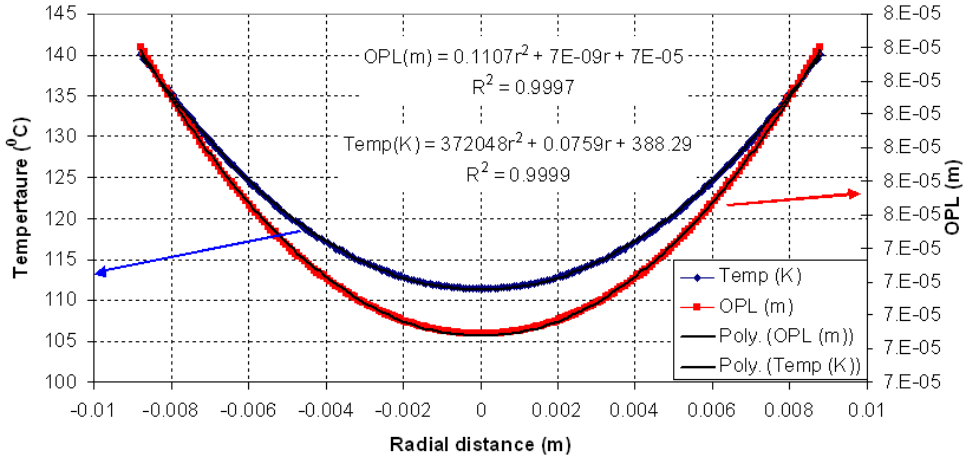

Fig. 15: Simulated temperature profile and the resultant OPL as a function of radial distance. Quadratic fits and the corresponding Regression coefficient is also shown.

3.6 Thermal depolarization

Optical birefringence can arise from heating-induced photoelastic stresses in glasses, resulting in thermal depolarization. This anisotropy can be an issue for polarization-sensitive experiments where depolarization is undesirable. To investigate this issue, we placed the SF57 between two crossed polarizers and measured the transmission of a specific polarization through the SF57 with no heating and with full heating. The results are summarized in Table 3, which shows that there is negligible thermal depolarization. The theoretical justification of this experimental result would be obtained by doing a photoelastic analysis of SF57. However, because the temperature-dependent stress-optical coefficient data for SF57 is not known, we are unable to complete such an analysis. In view of the experimental results above, we can say that, to the precision of the experiment, SF57 does not show any thermal depolarization.

Table 3: Thermal Depolarization Measurement Summary

State	Incident Polarization	Isolation ratio
No heating	s	-37.06 +/- 0.1
2.4 W heating per heater	s	-37.1 +/- 0.1
No heating	p	-30.60 +/- 0.1
2.4 W heating per heater	p	-30.60 +/-0.1

3.7 Coating reflectivity change

Another potential issue is the possible change in the reflectivity of SF57 when heated to high temperature. This change would be directly related to the quality of the anti-reflection (AR) coatings available. In these experiments, we used commercial off-the-shelf AR coating on both SF57 surfaces. These coatings were determined to have a reflectance of approximately 500 ppm per surface at room temperature. The reflectivity increased to 1000 ppm per surface at 200^0C. Potentially better coatings could be obtained if optical losses are an issue in a particular application or the coating could be designed for a specific working temperature.

5. Summary

In conclusion, we have demonstrated an adaptive beam shaping element that can change the beam shape effectively independently along two orthogonal axes. A focal length dynamic range of minus infinity to -10 m has been achieved by heating from room temperature to 200^0C. We have investigated beam steering, beam shape, beam quality, thermal depolarization, and reflectivity change as a function of temperature. The beam quality does not change significantly over this range of temperature. The proposed system was also tested for astigmatic lens creation. A differential lens of -10 m can be obtained by applying heating to one axis only. Another possible application of the system is its ability to be used for high-resolution, slow-speed beam steering.

This segmented heating system provides a powerful way to shape optical beams without the need for moving elements. It can be used in vacuum, where accessing and moving lenses proves difficult. The proposed system is particularly useful with high laser power systems where other alternatives like deformable mirrors, digital micro-mirror devices, and liquid crystals may not work. Another application of the proposed system is adaptive correction of high power thermal effects and an ability to correct astigmatism.

Acknowledgments

The authors acknowledge the encouragement of the LIGO Science Collaboration. Discussions with Volker Questchke, Rich Abbott, Peter Fritschel, and Dennis Coyne have been very helpful. This work is supported by the National Science Foundation under grant PHY-0855313.